A Journal of the Gesellschaft Deutscher Chemiker

Angewandte Chemie

GDCh

International Edition

www.angewandte.org

Accepted Article

Title: Revealing the A-site effect of lead-free A3Sb2Br9 perovskite in photocatalytic C (sp3)-H bonds activation

Authors: Zhenzhen Zhang, Yuying Yang, Yingying Wang, Lanlan Yang, Qi Li, Langxing Chen, and Dongsheng Xu

To be cited as: *Angew. Chem. Int. Ed.* 10.1002/anie.202005495

Link to VoR: https://doi.org/10.1002/anie.202005495

WILEY-VCH

10.1002/anie.202005495

WILEY-VCH

Revealing the A-site effect of lead-free $A_3Sb_2Br_9$ perovskite in photocatalytic C (sp^3)-H bonds activation

Zhenzhen Zhang,[a,b] Yuying Yang,[a] Yingying Wang,[a] Lanlan Yang,[a] Qi Li,*[a] Langxing Chen*[b] and Dongsheng Xu*[a]

Abstract: Lead-free halide perovskite of $A_3Sb_2Br_9$ is utilized as photocatalyst for the first time to C (sp^3)-H bonds activation. $A_3Sb_2Br_9$ nanoparticles ($A_3Sb_2Br_9$ NPs) with different ratios of Cs and MA show different photocatalytic activity for toluene oxidation and the photocatalytic performance is enhanced when increasing the amount of Cs. We reveal that the octahedron distortion caused by A-site cations can change the electronic property of X-site ions and further affect the electron transfer from toluene molecules to Br sites. After the regulation of A-site cations, the photocatalytic activity is higher with $A_3Sb_2Br_9$ NPs than that with some classic photocatalysts (TiO_2, WO_3 and CdS). The main active species involved in photocatalytic oxidation of toluene are photogenerated holes (h^+) and superoxide anions ($\bullet O_2^-$). The view of octahedron distortion by A-site cations affecting photocatalytic activity remains unique and is also a step forward for understanding more insights to halide-perovskite-based photocatalysis. This opinion of relations between octahedron distortion and photocatalysis can also guide the design of new photocatalytic systems involved in other halide perovskites.

In recent years, lead halide perovskites with ABX_3 stoichiometry (where A = monovalent cation, B = Pb^{2+} and X = halide anion), are demonstrated to be good photocatalysts because of their high extinction coefficients[1], optimal band gaps[2], low exciton binding energy[3] and excellent charge transport properties[4]. They have been successfully applied in several photocatalytic reactions, e.g. hydrogen generation[5], CO_2 reduction[6], dye degradation[7] and organic synthesis[8]. However, the photocatalysis involved in lead halide perovskites suffers from disadvantages of low efficiency, unsatisfied stability and severe toxicity of lead. To address these problems, lead-free perovskites, in which Pb^{2+} at B-site are substituted by In^{3+}, Bi^{3+}, Sb^{3+} or Sn^{4+}, have been widely investigated because of their lower toxicity and relatively higher stability[9]. Moreover, modifications of X-site[10] and B-site[11] ions are effective ways to optimize their bandgap structures for improving their visible-light absorption ability and redox ability of photogenerated holes and electrons. Besides, methods such as doping[12], cocatalyst immobilization[13], and semiconductor combinations[6b, 14] are also employed to improve the photocatalytic efficiency of halide perovskites.

It is widely accepted that A-site cations are rarely considered for the performance optimization of halide perovskite photocatalysts because they are not directly involved in the construction of the bandgaps[15]. Bhosale et al[16] reported that $Cs_3Bi_2I_9$ exhibited higher efficiency of carrier generation relative to $MA_3Bi_2I_9$ and $Rb_3Bi_2I_9$ in photocatalytic CO_2 reduction when irradiated by light at 305 nm. However, it is unclear that the holes and electrons are excited by either bandgap absorption of semiconductor or Bi-I transition under such high-energy UV light irradiation.

In this communication, we employed $A_3Sb_2Br_9$ perovskite nanoparticles (NPs) as a new photocatalyst into visible-light-driven photocatalytic C(sp^3)-H bonds activation, indicating that the photocatalytic activity is strongly related to the distortion of $[SbBr_6]$ octahedron affected by A-site cations. Theoretical calculation[17] indicates that $Cs_3Sb_2Br_9$ exhibits suitable band structure (conduction band position: -3.98 V; valence band position: -6.58 V *vs.* vacuum) and obvious difference of mobilities between holes and electrons, implying high oxidation ability of its holes and high efficiency of charge separation. In our experiments, $Cs_3Sb_2Br_9$ NPs presented stable and efficient photocatalytic ability for toluene oxidation to benzaldehyde. Interestingly, the photocatalytic activity with pure $Cs_3Sb_2Br_9$ NPs is about 5.3 times of that with $MA_3Sb_2Br_9$ NPs and the photocatalytic efficiency of $Cs_xMA_{3-x}Sb_2Br_9$ NPs increases with the increase of Cs ratio. X-ray photoelectron spectroscopy (XPS) characterizations indicate that the binding energies of Sb shift in the negative direction with the increase of the Cs^+ amount in $Cs_xMA_{3-x}Sb_2Br_9$ NPs. According to the photocatalytic performance, crystal structures and XPS results, we deduce that the change of octahedron distortion by A-site cations can affect the electronic property of Br active sites and lead to the disparity of the ability of electron transfer from toluene molecules to Br sites.

$A_3Sb_2Br_9$ NPs were synthesized by an anti-solvent recrystallization method. ABr (A=Cs or MA) and $SbBr_3$ were dissolved in good solvent of DMSO and quickly poured into a mixture of chloroform and oleic acid as poor solvent. As can be seen in Figure 1A, the size of $Cs_3Sb_2Br_9$ NPs is from tens of nanometers to hundreds of nanometers. In the HRTEM image of $Cs_3Sb_2Br_9$ NPs (Figure 1B), lattice fringes with 0.21, 0.31, and 0.40 nm spacing, corresponding to (302), (112) and (110) facets of $Cs_3Sb_2Br_9$, respectively, can be identified. The PXRD patterns of $Cs_xMA_{3-x}Sb_2Br_9$ NPs (Figure 1C), in which the x values were evaluated by ICP-AES (Table S1), display that their crystal structures are similar to that of $Cs_3Sb_2Br_9$ NPs and there is no obvious phase segregation. With the decrease of Cs^+ amount in $Cs_xMA_{3-x}Sb_2Br_9$ NPs, the peaks continually shift to small angles, attributing to the octahedron distortion by larger MA^+ ions.

[a] Dr. Z. Zhang, Y. Yang, Dr. Y. Wang, L. Yang, Prof. Dr. Q. Li, Prof. Dr. D. Xu
Beijing National Laboratory for Molecular Sciences, State Key Laboratory for Structural Chemistry of Unstable and Stable Species, College of Chemistry and Molecular Engineering, Peking University, Beijing 100871, China
E-mail address: liqi2010@pku.edu.cn
dsxu@pku.edu.cn
[b] Dr. Z. Zhang, Prof. Dr. L. Chen
Research Center for Analytical Sciences, College of Chemistry, Tianjin Key Laboratory of Biosensing and Molecular Recognition, State Key Laboratory of Medicinal Chemical Biology, Nankai University, Tianjin 300071, China
E-mail address: lxchen@nankai.edu.cn

10.1002/anie.202005495

Meanwhile, the optical absorption band edges of $Cs_xMA_{3-x}Sb_2Br_9$ NPs show a slight blue shift with the MA^+ increasing (Figure 1D). As the size of MA^+ is larger than that of Cs^+, the cell volume of $Cs_xMA_{3-x}Sb_2Br_9$ increases with the adding of MA^+, exhibiting larger bandgaps, in accordance with the reported result [15a].

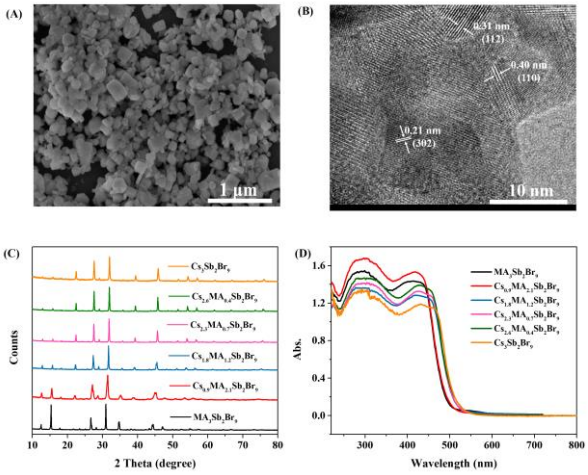

Figure 1. SEM image (A) and TEM image (B) of $Cs_3Sb_2Br_9$ NPs; PXRD patterns (C) and optical absorption spectra (D) of $Cs_xMA_{3-x}Sb_2Br_9$ NPs (x = 0-3)

To study the influence of A-site cations in $A_3Sb_2Br_9$ NPs on photocatalysis, photocatalytic oxidation of toluene was carried out with $Cs_xMA_{3-x}Sb_2Br_9$ NPs (x=0-3). The main products are benzaldehyde and benzyl alcohol, and their MS spectra are shown in Figure S1. The conversion rates of toluene oxidation are firstly enhanced and then dropped a little with the increase of Cs^+ (Figure 2A). The photocatalytic activity with pure $Cs_3Sb_2Br_9$ NPs is about 5.3 times of that with $MA_3Sb_2Br_9$ NPs, which cannot be attributed to the slight narrowing (ca. 0.13 eV, Figure S2A and S2B) of bandgaps. Meanwhile, the narrowing of bandgaps will lift the valance band positions (XPS valance band spectra in Figure S2C) and further lower the oxidation ability. In addition to toluene oxidation, $Cs_3Sb_2Br_9$ NPs are also efficient for photocatalytic C (sp^3)-H bonds activation in other substrates, e.g. 2-BT, 4-BT and cyclohexane (Table 1). Specially, for the photocatalytic oxidation of cyclohexane, cyclohexanol and cyclohexanone are produced, in contrast to single product of cyclohexanone for $FAPbBr_3$ photocatalyst[18]. To reveal the high activity of $Cs_3Sb_2Br_9$ NPs, photocatalytic experiments under monochromatic light irradiation were conducted (Figure 2B). The total amount of benzaldehyde and benzyl alcohol products at monochromatic light can be well fitted with the optical absorption spectrum of $Cs_3Sb_2Br_9$ NPs, indicating a photocatalytic oxidation mechanism. As shown in Figure S3, the photocatalytic toluene oxidation can be severely blocked by 2,2',6,6'-tetramethylpiperidine-1-oxyl (TEMPO), proving that the photocatalytic toluene oxidation is a free-radical-based process. Moreover, experiments with specific scavengers were conducted to verify the roles of various redox-active species, e.g., ammonium oxalate for holes (h^+), 1,4-benzoquinone for $\bullet O_2^-$ and t-butanol for •OH radicals. From Figure 2C, it can be found that the h^+ and $\bullet O_2^-$ have positive correlation with the conversion rate while •OH radicals are unaffected. The characteristic peaks of DMPO-$\bullet O_2^-$ adduct in the EPR spectra (Figure 2D) upon visible-light irradiation also proves the existence of $\bullet O_2^-$. All these results demonstrate that h^+ and $\bullet O_2^-$ are main active species in photocatalytic oxidation of toluene.

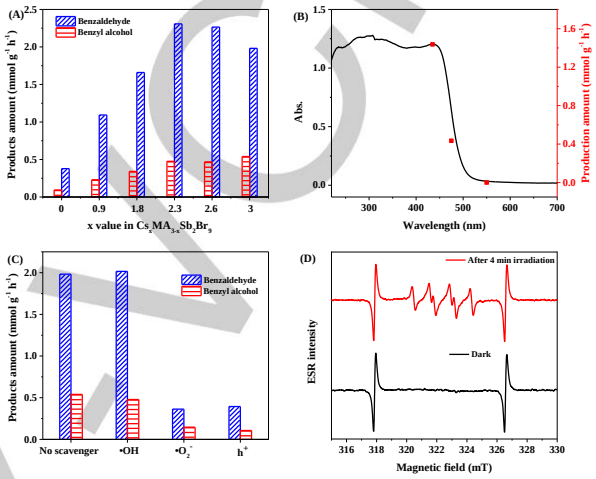

Figure 2. (A) Photocatalytic activity of toluene oxidation with $Cs_xMA_{3-x}Sb_2Br_9$ NPs (x = 0-3) photocatalysts; (B) Optical absorption spectrum of $Cs_3Sb_2Br_9$ NPs and the total production rates of benzaldehyde and benzyl alcohol at different monochromatic incident light irradiation (light intensity: 20 mW cm^{-2}; irradiation time: 1 h); (C) Photocatalytic activity of toluene oxidation in the absence or presence of various active species scavengers; (D) EPR spectra of DMPO-$\bullet O_2^-$ adduct in the dark (black curve) and under the irradiation of visible light for 4 min (red curve)

Table 1 Photo-oxidation of hydrocarbons over $Cs_3Sb_2Br_9$ NPs photocatalyst under visible light irradiation in O_2 atmosphere [a]

Substrates [b]	Products [c]	Production rate (mmol g^{-1} h^{-1})
Toluene	Benzaldehyde	1.98
	Benzyl alcohol	0.54
c-Hexane	c-Hexanol	0.70
	c-Hexanone	0.28
2-BT	2-BBD	1.76
	2-BBA	0.52
4-BT	4-BBD	2.07
	4-BBA	0.50

[a] Reaction conditions: 5 mL liquid hydrocarbon, 10 mg $Cs_3Sb_2Br_9$ NPs as photocatalyst, 1 atm O_2 at room temperature under visible light (λ＞420 nm) irradiation, reaction time: 4 h

[b] c-Hexane: cyclohexane; 2-BT: 2-bromotoluene; 4-BT: 4-bromotoluene

[c] c-Hexanol: cyclohexanol; c-Hexanone: cyclohexanone; 2-BBD: 2-bromobenzaldehyde; 2-BBA: 2-bromobenzyl alcohol; 4-BBD: 4-bromobenzaldehyde; 4-BBA: 4-bromobenzyl alcohol

To elucidate the mechanism of A-site effect in the above photocatalytic processes, XPS analysis of $Cs_xMA_{3-x}Sb_2Br_9$ NPs

was performed (Figure S4 and Figure 3). In general, A-site cations can cause the octahedron distortion in halide perovskites due to Jahn-Teller effect and further affect the crystal field splitting energy of the central ions at B-sites. In Figure 3, the binding energy of Sb 4d shifts negatively gradually as the increase of x value in $Cs_xMA_{3-x}Sb_2Br_9$ NPs. In contrast, the binding energies of N 1s, Cs 3d and Br 3d have no obvious change (Figure S4). This indicates that Sb elements become electron richer with the decrease of MA^+ amount and Br subsequently should be electron deficient to certain extent.

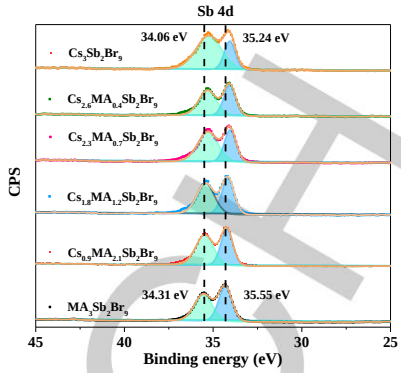

Figure 3. High-resolution XPS spectra of Sb 4d for $Cs_xMA_{3-x}Sb_2Br_9$ NPs (x=0-3).

Based on the analysis above, we propose the mechanisms of both photocatalytic C (sp^3)-H bonds activation and the A-site effect in $A_3Sb_2Br_9$, as shown in Figure 4. Firstly, h^+ and e^- are generated on the surface of $A_3Sb_2Br_9$ photocatalyst under visible light irradiation. Then, photogenerated h^+ oxidize toluene to benzyl radicals, which is usually regarded as the rate-determing step[19]; meawhile, photogenerated e- reduce O_2 to $\bullet O_2^-$. Benzyl radicals and $\bullet O_2^-$ can react with each other to form benzaldehyde and OH^-, then OH^- further reacts with protons on the surface of $A_3Sb_2Br_9$ NPs to produce H_2O molecules. During the above process, Br sites are responsible for the generation of h^+ and the breaking of C-H bonds[20]. Hence, the electronic properties of Br atoms on the surface can tremendously affect the activity of toluene oxidation. As we can see in Figure 4B, three Sb-Br bonds become shorter and the other three become longer for the $MA_3Sb_2Br_9$ octahedron, compared to that for $Cs_3Sb_2Br_9$ octahedron (the data are obtained from the crystallographic information files of ICSD-39824 for $Cs_3Sb_2Br_9$ and ICSD-110339 for $MA_3Sb_2Br_9$). In other words, there has octahedron distortion for $MA_3Sb_2Br_9$. The octahedron distortion can be reflected by the values of c/a in unit cells and smaller c/a means larger distortion in the case of $A_3Sb_2Br_9$. From Figure S5 (c/a values were calculated from the PXRD data), we can see that the octahedron distortion of $Cs_xMA_{3-x}Sb_2Br_9$ becomes larger with the increase of MA amount. Combining the XPS results and crystal structures, we believe that electron cloud density of Br sites on the surface of $A_3Sb_2Br_9$ increases when Cs are replaced by MA and results in decreasing the ability on the weakening of C-H bonds.

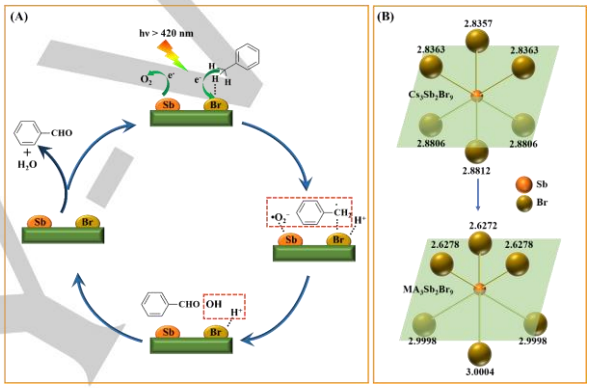

Figure 4. Possible mechanism of A-site effect on C (sp^3)-H bonds activation: (A) photocatalytic process of toluene oxidation; (B) octahedron distortion caused by A-site cations

Moreover, this A-site effect can be extended to direct the design of new photocatalytic systems involved in other halide perovskites. On one hand, for the oxidation reactions occurred at X-site, the octahedron distortion related to A-site cations can make X-site ions electron richer and lower the oxidation ability of X-site ions. Similar results were observed for perovskite oxides-based photocatalysis.[21] In our experiments, the photocatalytic activity with $Cs_3Sb_2Br_9$ NPs is about 20.7, 7.8 and 4.1 times of that with CdS NPs, WO_3 NPs and P25, respectively (Figure S6). On the other hand, for reduction reactions at B-sites like hydrogen evolution reaction[10], octahedron distortion is also not beneficial for photocatalytic reactions because of the decrease of electron cloud density at B-sites. In addition, octahedron distortion by A-site cations can also affect the photocatalytic stability of halide perovskites because of their weaker chemical stability and lower electron consumption rate. As shown in Figure S7, over 80% photocatalytic efficiency retained after four times of cycling for $Cs_3Sb_2Br_9$ NPs with higher stability. The main structure was preserved after four cycles of reaction, and the appearance of CsBr peaks in PXRD pattern might be responsible for the decrease of photocatalytic activity during the long-time reactions (Figure S8-11).

In conclusion, lead-free $A_3Sb_2Br_9$ perovskites were applied in photocatalytic applications for the first time and high

photocatalytic activity for C (sp^3)-H bond activation was obtained. The main redox-active species are photogenerated holes and superoxide anions. More importantly, it is demonstrated that A-site cations in halide perovskites have significant effect on the photocatalytic efficiency and the increase of Cs^+ amount in $Cs_xMA_{3-x}Sb_2Br_9$ photocatalyst can obviously enhance the photocatalytic performance. We reveal that the octahedron distortion affected by A-site cations can change electronic properties of Br active sites and further vary the photocatalytic capacity. This work would provide new insight for the A-site effect in halide perovskite photocatalysis and pave new ways for designing highly efficient halide perovskite photocatalysts.

Acknowledgements

This work was supported by the National Natural Science Foundation of China (grant No. 21821004).

Keywords: Lead-free Perovskites • A-site effect • Photocatalysis • C-H bonds activation • Jahn-Teller distortion

[1] S. Kazim, M. K. Nazeeruddin, M. Gratzel, S. Ahmad, *Angew. Chem. Int. Ed.* **2014**, *53*, 2812-2824.

[2] M. R. Filip, G. E. Eperon, H. J. Snaith, F. Giustino, *Nat. Commun.* **2014**, *5*, 5757-5765.

[3] S. Kazim, M. K. Nazeeruddin, M. Gratzel, S. Ahmad, *Angew. Chem. Int. Ed*. **2014**, *53*, 2812-2824.

[2] M. R. Filip, G. E. Eperon, H. J. Snaith, F. Giustino, *Nat. Commun.* **2014**, *5*, 5757-5765.

[3] W. Du, S. Zhang, Q. Zhang, X. Liu, *Adv. Mater.* **2018**, 1804894-1804899.

[4] S. D. Stranks, G. E. Eperon, G. Grancini, C. Menelaou, M. J. Alcocer, T. Leijtens, L. M. Herz, A. Petrozza, H. J. Snaith, *Science* **2013**, *342*, 341-344.

[5] a) S. Park, W. J. Chang, C. W. Lee, S. Park, H.-Y. Ahn, K. T. Nam, *Nat. Energy* **2016**, *2*, 16185-16192; b) Y. Wu, P. Wang, X. Zhu, Q. Zhang, Z. Wang, Y. Liu, G. Zou, Y. Dai, M. H. Whangbo, B. Huang, *Adv. Mater.* **2018**, *30*, 1704342-1704347; c) M. Wang, Y. Zuo, J. Wang, Y. Wang, X. Shen, B. Qiu, L. Cai, F. Zhou, S. P. Lau, Y. Chai, *Adv. Energy Mater.* **2019**, *9*, 1901801-1901807.

[6] a) Y. F. Xu, M. Z. Yang, B. X. Chen, X. D. Wang, H. Y. Chen, D. B. Kuang, C. Y. Su, *J. Am. Chem. Soc.* **2017**, *139*, 5660-5663; b) M. Ou, W. Tu, S. Yin, W. Xing, S. Wu, H. Wang, S. Wan, Q. Zhong, R. Xu, *Angew. Chem. Int. Ed.* **2018**, *57*, 13570-13574; c) L. Y. Wu, Y. F. Mu, X. X. Guo, W. Zhang, Z. M. Zhang, M. Zhang, T. B. Lu, *Angew. Chem. Int. Ed.* **2019**, *58*, 9491-9495.

[7] a) S. Saris, A. Loiudice, M. Mensi, R. Buonsanti, *J. Phys. Chem. Lett.* **2019**, *10*, 7797-7803; b) A. F. Gualdron-Reyes, J. Rodriguez-Pereira, E. Amado-Gonzalez, P. J. Rueda, R. Ospina, S. Masi, S. J. Yoon, J. Tirado, F. Jaramillo, S. Agouram, V. Munoz-Sanjose, S. Gimenez, I. Mora-Sero, *ACS. Appl. Mater. Interfaces* **2020**, *12*, 914-924.

[8] a) K. Chen, X. Deng, G. Dodekatos, H. Tuysuz, *J. Am. Chem. Soc.* **2017**, *139*, 12267-12273; b) H. Huang, H. Yuan, K. P. F. Janssen, G. Solís-Fernández, Y. Wang, C. Y. X. Tan, D. Jonckheere, E. Debroye, J. Long, J. Hendrix, J. Hofkens, J. A. Steele, M. B. J. Roeffaers, *ACS Energy Lett.* **2018**, *3*, 755-759; c) X. Zhu, Y. Lin, J. San Martin, Y. Sun, D. Zhu, Y. Yan, *Nat. Commun.* **2019**, *10*, 2843-2852.

[9] a) J. Luo, X. Wang, S. Li, J. Liu, Y. Guo, G. Niu, L. Yao, Y. Fu, L. Gao, Q. Dong, C. Zhao, M. Leng, F. Ma, W. Liang, L. Wang, S. Jin, J. Han, L. Zhang, J. Etheridge, J. Wang, Y. Yan, E. H. Sargent, J. Tang, *Nature* **2018**, *563*, 541-545; b) M. Leng, Z. Chen, Y. Yang, Z. Li, K. Zeng, K. Li, G. Niu, Y. He, Q. Zhou, J. Tang, *Angew. Chem. Int. Ed.* **2016**, *55*, 15012-15016; c) F. Jiang, D. Yang, Y. Jiang, T. Liu, X. Zhao, Y. Ming, B. Luo, F. Qin, J. Fan, H. Han, L. Zhang, Y. Zhou, *J. Am. Chem. Soc.* **2018**, *140*, 1019-1027; dA. Wang, X. Yan, M. Zhang, S. Sun, M. Yang, W. Shen, X. Pan, P. Wang, Z. Deng, *Chem. Mater.* **2016**, *28*, 8132-8140.

[10] a) Y. Wu, P. Wang, Z. Guan, J. Liu, Z. Wang, Z. Zheng, S. Jin, Y. Dai, M.-H. Whangbo, B. Huang, *ACS Catal.* **2018**, *8*, 10349-10357; b) Z. Guan, Y. Wu, P. Wang, Q. Zhang, Z. Wang, Z. Zheng, Y. Liu, Y. Dai, M.-H. Whangbo, B. Huang, *Appl. Catal., B* **2019**, *245*, 522-527.

[11] Y. Dai, H. Tuysuz, *ChemSusChem* **2019**, *12*, 2587-2592.

[12] a) C. Tang, C. Chen, W. Xu, L. Xu, *J. Mater. Chem. A* **2019**, *7*, 6911-6919; b) S. Shyamal, S. K. Dutta, N. Pradhan, *J. Phys. Chem. Lett.* **2019**, 7965-7969.

[13] Z.-C. Kong, H.-H. Zhang, J.-F. Liao, Y.-J. Dong, Y. Jiang, H.-Y. Chen, D.-B. Kuang, *Sol. RRL* **2019**, *4*, 1900365-1900371.

[14] a) Z. Zhao, J. Wu, Y.-Z. Zheng, N. Li, X. Li, X. Tao, *ACS Catal.* **2019**, *9*, 8144-8152; b) Y.-C. Pu, H.-C. Fan, T.-W. Liu, J.-W. Chen, *J. Mater. Chem. A* **2017**, *5*, 25438-25449.

[15] a) J. S. Manser, J. A. Christians, P. V. Kamat, *Chem. Rev.* **2016**, *116*, 12956-13008; b) J. Liang, D. Chen, X. Yao, K. Zhang, F. Qu, L. Qin, Y. Huang, J. Li, *Small* **2019**, 1903398-1903417.

[16] S. S. Bhosale, A. K. Kharade, E. Jokar, A. Fathi, S. M. Chang, E. W. Diau, *J. Am. Chem. Soc.* **2019**, *141*, 20434-20442.

[17] Y.-L. Liu, C.-L. Yang, M.-S. Wang, X.-G. Ma, Y.-G. Yi, *J. Mater. Sci.* **2018**, *54*, 4732-4741.

[18] H. Huang, H. Yuan, J. Zhao, G. Solís-Fernández, C. Zhou, J. W. Seo, J. Hendrix, E. Debroye, J. A. Steele, J. Hofkens, J. Long, M. B. J. Roeffaers, *ACS Energy Lett.* **2018**, *4*, 203-208.

[19] X. Cao, Z. Chen, R. Lin, W.-C. Cheong, S. Liu, J. Zhang, Q. Peng, C. Chen, T. Han, X. Tong, Y. Wang, R. Shen, W. Zhu, D. Wang, Y. Li, *Nat. Catal.* **2018**, *1*, 704-710

[20] Y. Dai, C. Poidevin, C. Ochoa-Hernandez, A. Auer, H. Tuysuz, *Angew. Chem. Int. Ed.* **2019**, *59*, 5788-5796.

[21] S. Rani, G. Naresh, T. K. Mandal, *Dalton Trans*. **2020**, *49*, 1433-1445.

10.1002/anie.202005495

WILEY-VCH

Entry for the Table of Contents

COMMUNICATION

$A_3Sb_2Br_9$ nanoparticles (NPs) with different ratios of Cs and MA were employed into photocatalytic C (sp^3)-H bonds activation with high conversion rates. It was demonstrated that the octahedron distortion by A-site cations could affect the electronic property of $A_3Sb_2Br_9$ and further influence the photocatalytic activity.

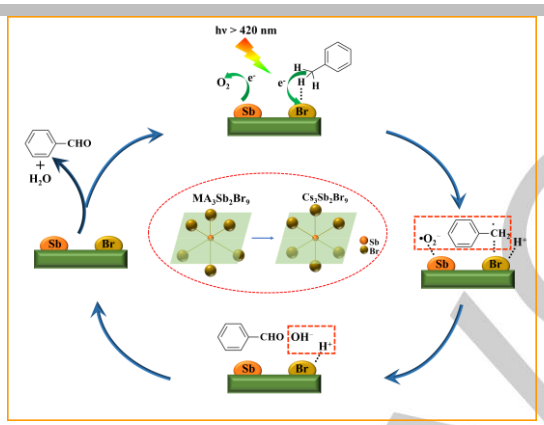

Zhenzhen Zhang[a, b], Yuying Yang[a], Yingying Wang[a], Lanlan Yang[a], Qi Li[a], Langxing Chen[b]*, Dongsheng Xu[a]**

Page No. – Page No.

Revealing the A-site effect of lead-free $A_3Sb_2Br_9$ perovskite in photocatalytic C (sp^3)-H bonds activation